

## Article

# Assessment of Tube–Fin Contact Materials in Heat Exchangers: Guidelines for Simulation and Experiments

László Budulski <sup>1</sup>, Gábor Loch <sup>1</sup>, László Lenkovic <sup>1</sup>, Mihály Baumann <sup>1</sup>, Balázs Cakó <sup>1</sup>, Tamás Zsebe <sup>2</sup>, Zoltán Meiszterics <sup>2</sup>, Gyula Ferenc Vasvári <sup>2</sup>, Boldizsár Kurilla <sup>2</sup>, Tamás Bitó <sup>2</sup>, Géza György Várady <sup>3</sup> and Dávid Csonka <sup>2,\*</sup>

- <sup>1</sup> Department of Building Services and Building Engineering, Faculty of Engineering and Information Technology, University of Pécs, 7624 Pécs, Hungary; budulskil@mik.pte.hu (L.B.); loch.gabor@mik.pte.hu (G.L.); lenkovic.laszlo@mik.pte.hu (L.L.); baumann.mihaly@mik.pte.hu (M.B.); cako.balazs@mik.pte.hu (B.C.)
- <sup>2</sup> Department of Mechanical Engineering, Faculty of Engineering and Information Technology, University of Pécs, 7624 Pécs, Hungary; zsebe.tamas@mik.pte.hu (T.Z.); meiszterics.zoltan@mik.pte.hu (Z.M.); vasvari.gyula@mik.pte.hu (G.F.V.); kurilla.boldizsar@mik.pte.hu (B.K.); bito.tamas@mik.pte.hu (T.B.)
- <sup>3</sup> Autonomous Technologies and Drones Research Team, Faculty of Engineering and Information Technology, University of Pécs, 7624 Pécs, Hungary; varady.geza@mik.pte.hu
- \* Correspondence: csonka.david@mik.pte.hu

**Abstract:** This paper describes experiments on finned tube heat exchangers, focusing on reducing the thermal contact resistance at the contact between the pipe and the lamella. Various contact materials, such as solders and adhesives, were investigated. Several methods of establishing contact were tested, including blowtorch soldering, brazing, and furnace soldering. Thermal camera measurements were carried out to assess the performance of the contact materials. Moreover, finite element analysis was performed to evaluate the contact materials and establish guidelines in the fin–tube connection modeling by comparing simplified models with the realistic model. Blowtorch brazing tests were successful while soldering attempts failed. During the thermographic measurements, reflective surfaces could be measured after applying a thin layer of paint with high emissivity. These measurements did not provide valuable results; thus, the contact materials were assessed using a finite element analysis. The results from the finite element analysis showed that all the inspected contact materials provided better heat transfer than not using a contact material. The heat transfer rate of the tight-fit realistic model was found to be 33.65 for air and 34.9 for the Zn-22Al contact material. This finding could be utilized in developing heat exchangers with higher heat transfer with the same size.

**Keywords:** heat exchanger; contact material; thermal conductivity; soldering; brazing; thermal resistance; thermal imaging; finite element analysis



**Citation:** Budulski, L.; Loch, G.; Lenkovic, L.; Baumann, M.; Cakó, B.; Zsebe, T.; Meiszterics, Z.; Vasvári, G.F.; Kurilla, B.; Bitó, T.; et al. Assessment of Tube–Fin Contact Materials in Heat Exchangers: Guidelines for Simulation and Experiments. *Energies* **2024**, *17*, 5681. <https://doi.org/10.3390/en17225681>

Academic Editors: Artur Blaszczyk, Tadeusz Bohdal and Marcin Kruzel

Received: 30 September 2024  
Revised: 1 November 2024  
Accepted: 9 November 2024  
Published: 13 November 2024



**Copyright:** © 2024 by the authors. Licensee MDPI, Basel, Switzerland. This article is an open access article distributed under the terms and conditions of the Creative Commons Attribution (CC BY) license (<https://creativecommons.org/licenses/by/4.0/>).

## 1. Introduction

In present industrial technology, heat exchangers are indispensable parts of various industries and applications, from HVAC systems to power plants. Among the diverse types of heat exchangers available, finned tube heat exchangers have attracted attention for their efficiency and versatility [1,2]. However, plenty of room for improvement remains. A promising area of development is the contact quality between the tube and the fin [3]. Relevant literature is very scarce in this area, but it is proven that proper contact is required for low thermal contact resistance [4,5]. Spiral-fin tube heat exchangers can be welded [6], but that is not the case for fin–tube heat exchangers. Currently, the method of production of these copper–aluminum heat exchangers, which is the most widespread material combination used, excludes using any bonding methods between the fin and the pipe. The connection is usually instituted by pulling a bullet through the pipes, thus expanding their walls onto the fin collars to attain a tight metal-to-metal contact between

the two [7–9]. Press-fitting presents disadvantages, however, including a substandard fit ascribed to surface voids, the presence of contaminants, material defects on the surface, and undesired ductile distortions, such as warping or the breaking of fin collars during the tube expansion process [10]. In bimetallic configurations, loosening of the fins may occur due to an increasing temperature caused by varying degrees of thermal expansion between the two materials, different stages of fatigue caused by thermal cycling, or surface roughness. The temperature discontinuity due to contact resistance is widely known [11].

This study investigates the potential methods for improving pipe–fin contact, focusing on the evaluation of different contact materials concerning thermal conduction in comparison to conventional press-fitting techniques. The research initially examined the solderability and brazeability of commonly used materials, such as those found in aluminum-finned copper pipe heat exchangers, which are universally utilized in HVAC systems both industrially and domestically. Additionally, heat-conducting adhesives were tested as prospective interface materials. This study provides an in-depth analysis of the challenges encountered during the production of test specimens and measurements and discusses the results of thermal tests performed on the selected materials. Thermal testing of filler metals for soldering and brazing was deemed necessary to validate the thermal properties specified in their data sheets and to assess the accuracy of temperature control in the electric furnace used. Potential opportunities are considered for future research to improve the effectiveness of finned tube heat exchangers.

In this research, thermal imaging is highlighted as a key inspection method. Generally, image processing in thermal imaging cameras is divided into three categories of methods and algorithms. The first category includes algorithms essential for the thermal imaging camera's operation, such as correcting detector response unevenness in FPA [1,2] and triggering signals from faulty detectors. The second category comprises algorithms designed to enhance image quality, thereby enabling or facilitating thermal image interpretations by operators or vision systems. The third category consists of data analysis methods used for the automatic detection and tracking of objects within the image, as well as for scene interpretation.

The algorithms and processing methods in the first category are based on infrared detector system operations and the fundamental laws of infrared radiation. Key processing algorithms include correcting response mismatches among detectors in the array and identifying and replacing damaged detectors. Various algorithms address detector response mismatches, with the most widely used being single and two-point correction methods [12,13].

Thermal images typically depict the infrared radiation emitted by the observed object and its surroundings, and these thermal scenes look quite different from those captured by video cameras. Consequently, interpreting thermal images can be challenging. Accurate interpretation requires a sound understanding of infrared radiation properties, as well as specific object characteristics and the surrounding environment. During the perception process, both objective factors, such as an object's emission factor, and subjective factors, such as human visual perception, play significant roles [14]. However, merely setting optimal infrared camera parameters (like sharpness and temperature range) does not guarantee accurate perception and interpretation.

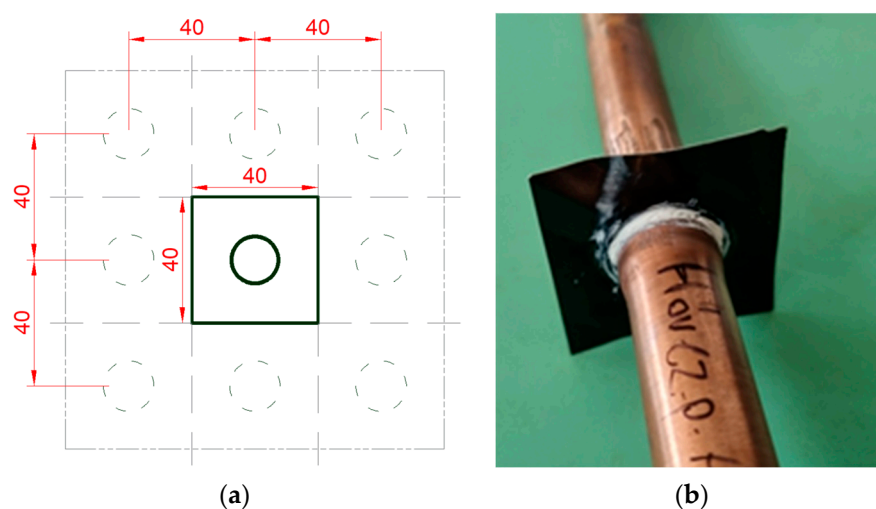
In this study, one of the primary tools utilized is finite element analysis (FEA), a critical computational technique within the field of engineering. FEA is employed to simulate and analyze intricate structures by discretizing them into smaller, finite elements, thereby enabling detailed examination of their behavior under various conditions. This technique solves partial differential equations governing phenomena such as stress distribution and heat transfer. FEA has become indispensable for predicting the performance and reliability of complex systems in engineering and is thus widely used in the research of heat exchangers [15–19]. The modeling of heat exchangers poses some widely known meshing difficulties [20], which come from the dimension difference of the thin lamellae and other volumes. Thus, another aim of this research is to establish some guidelines for modeling the fin–tube contact region of heat exchangers for a specified purpose.

## 2. Materials and Methods

Contact material research aimed to improve a lamella's heat transfer on an applicable copper tube. Different contact materials were used in the experiments.

To carry out the measurements, standard 5/8" nominal diameter Cu-DHP copper tubes of 25 cm length were manufactured from tubes supplied by CAADEX (Mindszentgodisa, Hungary), with a lamella placed in the middle. The connection between the lamella and the tube was made using various contact materials and manufacturing techniques (gluing, soldering, etc.). Two types of lamellae were supplied by CAADEX, both of the Al 8006 alloy, the difference being that one was an uncoated aluminum lamella, and the other was the same type of lamella but coated.

From the received lamella plates, smaller-sized lamellae were cut out, which was the optimized size for the modeling, i.e., they were cut out smaller at the pipe centers with a pipe joint, as demonstrated by Figure 1a, with a finished measurement specimen shown in Figure 1b.



**Figure 1.** (a) Dimensions of the lamellae prepared for testing; (b) The formed lamella fixed with contact material.

The grade of the joining and the heat transfer efficiency were assessed using thermal camera measurements and FEA.

### 2.1. Contact Materials and Applying Them

Based on Ref. [21], and after consultations with experts, contact materials were selected for the research. These consisted of four solders, a heat-conducting adhesive, and a brazing filler metal. A bottle of Inoflux brand soldering flux was also procured, which is stated to be used for the application of a wide range of metals, including aluminum, stainless steel, iron, brass, and copper.

Sn-4Ag solder and Loctite SI5404 adhesive materials were provided by manufacturers free of charge for research purposes, denoted by a \* in Table 1, which shows the relevant properties of all inspected contact materials.

For brazing, a Rothenberger LPG handheld blowtorch was used with nominal and operating temperatures of 1800 °C and 650 °C, and soldering was attempted with the mentioned device, as well as a Hőker 4/1230 programmable industrial electric oven with a peak power of 7 kW. For the tests in the furnace, the pipe and fin were kept upright by supports. For soldering and brazing, the pipe was secured in place by a V125-type parallel vise.

A thin layer of heat-conducting adhesive was applied on the surface of the middle section of the pipe, and then a fin piece was secured to it. After the removal of the excess adhesive, the test piece was left on a horizontal stand to solidify before curing.

**Table 1.** Properties of inspected contact materials.

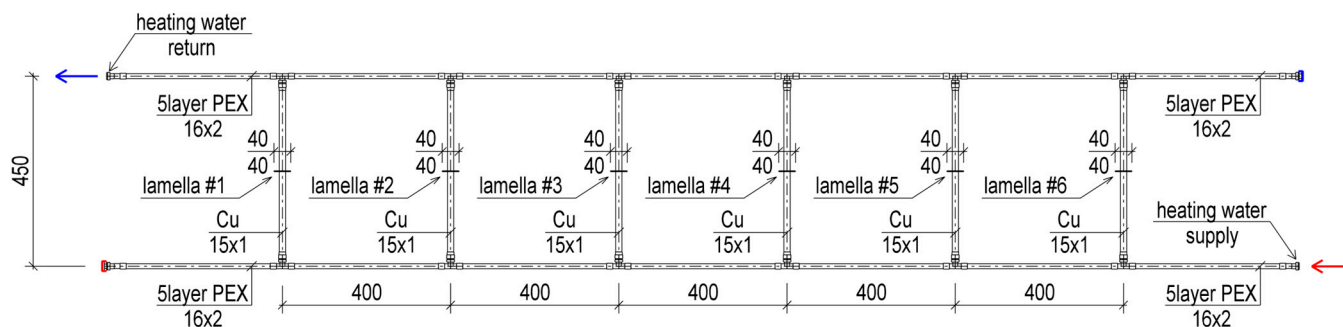
Contact Material	Sn-40Pb	Sn-4Ag *	SAC-305	Zn-22Al	Sn-9Zn	Loctite SI5404 *
Type of contact material	solder	solder	solder	filler metal for brazing	solder	adhesive
Composition	Sn 60% Pb 40%	Sn 96% Ag 4%	Sn 96.5% Ag 3% Cu 0.5%	Zn 78% Al 22%	Sn 91% Zn 9%	N/A
Density [kg/m <sup>3</sup> ]	8900	7400	7400	5250	7300	2400
Specific heat capacity (C <sub>p</sub> ) [J/kg·K]	180	220	220	~420	240	est. 800
Thermal conductivity [W/m·K]	~50	~78	58	125	61	≥0.95 LMS
Supplier	-	Castolin Zrt. (Pécs, Hungary)	Szinker Ltd. (Budapest, Hungary)	SolderWeld Inc. (Spanish Fork, UT, USA)	Szinker Ltd. (Budapest, Hungary)	Henkel Hungary Kft. (Budapest, Hungary)

\* materials were provided by manufacturers free of charge for research purposes.

A heating experiment was conducted on the solders to verify their melting points, or solidus-liquidus temperatures, as well as their behavior under elevated temperatures. Therefore, small solder pieces were put on fin material pieces and placed in the electric furnace one by one, which was preheated to just under the solidus of the material being tested, then raising the temperature by 5–10 °C and keeping it for 1–2 min before checking. This process was repeated until the test piece was in a liquid form.

## 2.2. Thermal Camera Measurements

Initially, thermocouple measurements [22] were attempted, but there were problems with the fixture, and the environmental effects caused inaccuracies. Thus, thermocouple temperature measurement was replaced by a thermographic solution. In the measuring loop, the fin measurements were carried out in parallel, with the fin and tube connected in a Tichelmann system to ensure uniform conditions, as shown in Figure 2. The measuring loop was insulated to maintain a constant and uniform temperature. A vacuum chamber could be effectively utilized [23], but that would exclude air side effects.

**Figure 2.** Lamella measurement setup in a Tichelmann system.

By using contact materials, heat transfer may be improved, in which case the fin temperature would increase; thus, a thermographic measurement is used. The instrument used was a Testo 882 thermal imaging camera (Testo Inc., Sparta, NJ, USA). The camera's sensitivity does not determine the accuracy of the temperature measurement, as it is determined by the emissivity factor of the inspected surface in addition to the measurement accuracy of the thermal camera. We can usually determine the emissivity with a lower accuracy.

The measurements' design is based on circulating heating water at a constant temperature in the tubes to ensure the same conditions between the different lamellae. The system was running with high-temperature water as far as possible so that larger differences could be detected. The principle of measuring contact materials is based on comparing the evolution of surface temperatures.

### 2.3. Finite Element Analysis

The finite element analysis had two main goals. One of them was to find the lamella shape in the contact region that can be optimally used in the simulations. The other goal was to compare different contact materials with each other and with the air gap.

The study aimed to compare models and materials proportionally with each other, not to calculate actual heat transfers. For this reason, significant simplifications have been made in the modeling. Therefore, an axisymmetric simulation environment was used. This greatly speeds up the calculation and does not require the meshing of volumes, thus allowing a much more detailed geometry and finer meshes while the simulation still runs relatively quickly. Inspecting only one lamella instead of modeling a whole heat exchanger is a great simplification but allows the aimed comparison. It does not matter that the calculated heat transfer is small; for a proportional comparison, a model with 100 lamellae would not be better. For measurement, it would be a problem because such a small value cannot be measured, but it is not an issue for calculation. In an axisymmetric model, the direction of the airflow cannot be correctly provided; thus, it is neglected.

Finite element analysis was carried out using AnSYS 2023 R2 and Fluent 23.2.0. For this study, turbulence was not the focus, so there was no need for complex turbulence models, but a laminar model provides unrealistic results, so the  $k$ - $\omega$  shear stress transport (SST) turbulence model was chosen.

This turbulence model is based on the Wilcox model [24] but refined in a way that it is less sensitive outside the shear layer. It employs a blending function to add the  $k$ - $\omega$  model of the near-wall region and the  $k$ - $\epsilon$  model of the far-field, the same as in the baseline (BSL) model [25]. Apart from this, the modeling constants are also different, and the transport of the turbulence shear stress is taken into account. Thus, the SST  $k$ - $\omega$  model is more robust and accurate for various flows.

The water flow has  $Re \sim 24,000$ , so it can be considered fully turbulent. The simulation conducted in this study was performed under steady-state conditions. At every wall boundary of the model, the condition is no slip, so the fluid boundary layer velocity is zero at the wall relative to it. Therefore, the heat flux can be calculated using Fourier's Law. The convection heat flux can be calculated using Newton's law of cooling. These fluxes are equal near the wall, and the flux balance is maintained; thus [26],

$$q_x'' = h(T_1 - T_2) = -k \frac{\partial T}{\partial x}$$

where  $T_1$  is the wall's temperature of the wall,  $T_2$  is the temperature of the fluid,  $k$  is the heat conductivity and  $h$  is the local heat transfer coefficient. The total heat transfer rate can be provided:

$$q = \bar{h} * A * (T_1 - T_2)$$

where  $A$  is the total surface area and  $\bar{h}$  is the area-averaged heat transfer coefficient.

From the heat flux balance, the general form of the equation of the heat transfer can be provided for the simplified geometry:

$$\frac{d^2 T}{dx^2} + \left( \frac{1}{A_C} \frac{dA_C}{dx} \right) \frac{dT}{dx} - \left( \frac{1}{A_C} \frac{h}{k} \frac{dA_S}{dx} \right) (T_1 - T_2) = 0$$

where  $A_C = A_C(x)$  is the cross-sectional area,  $A_S = A_S(x)$  is the surface area of the fins varying by distance.

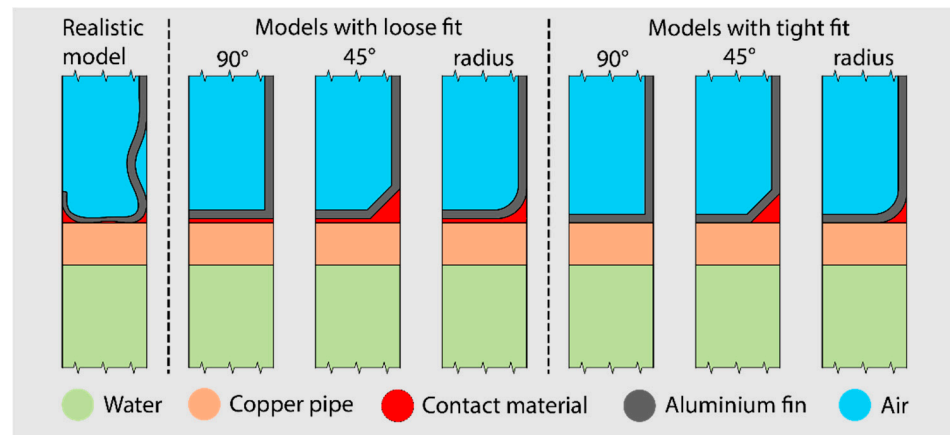
AnSYS Fluent uses the following energy equation:

$$\frac{\partial}{\partial t} \left[ \rho \left( e + \frac{v^2}{2} \right) \right] + \nabla \cdot \left[ \rho v \left( h + \frac{v^2}{2} \right) \right] = \nabla \cdot \left( k_{eff} \nabla T - \sum_j h_j \bar{J}_j + \bar{\tau}_{eff} \vec{v} \right) + S_h$$



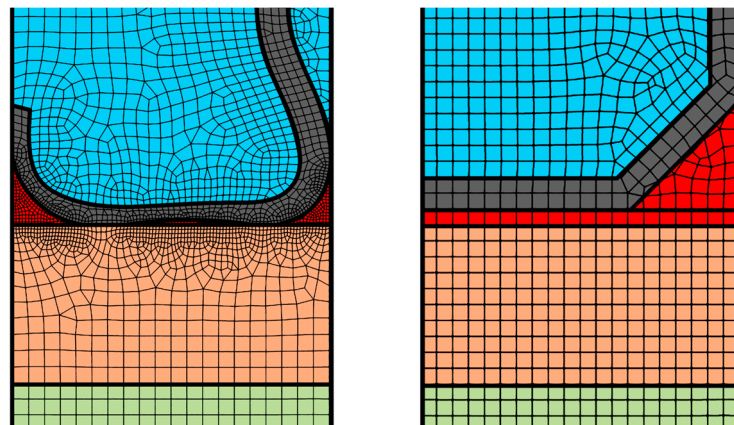
where  $k_{eff}$  is the effective conductivity depending on the turbulence model used, so  $k_{eff} \nabla T$  represents energy transfer due to conduction,  $\bar{J}_j$  is the diffusion flux, and  $\bar{\tau}_{eff} \vec{v}$  is viscous dissipation.  $S_h$  are volumetric heat sources, in the case of the current study, the radiation source.

To optimize computational efficiency, the simulation employed 2D axisymmetric models (Figure 3) to simplify the geometry while maintaining the ability to utilize a fine mesh.



**Figure 3.** Contact models for FEA.

The finite element mesh was created with a 0.1 mm maximum element size and a 1.2 growth rate. For the realistic model, a mesh refinement with a 0.02 mm and 0.05 mm element size was applied for the contact material gap and the aluminum fin, respectively. This was necessary because of the complex geometry of the realistic model. Figure 4 shows the mesh image of the realistic and the 45° loose fit models.



**Figure 4.** Mesh images of the contact regions of the realistic and the 45° loose fit models.

The inlet boundary condition of the fluid used in the copper pipe was water at 48 °C, flowing at a velocity of 1.5 m/s, with a pressure outlet at the exit. The air domain boundaries are pressure outlets, allowing the air to flow freely. The fin had a diameter of 200 mm, and the model incorporated a single fin per simulation. It is important to note that this setup does not reflect realistic conditions; rather, it was specifically designed to compare different tube–fin contact geometries. An idealized model was created under hypothetical factory conditions where there is no gap between the tube and the fin, except at the radius of the fin. The total heat transfer rates obtained from these idealized conditions were then compared to those from more realistic contact models. This comparative analysis aims to

provide insights into how aging and the associated increase in the tube–fin contact gap would proportionally reduce the total heat transfer rate over time.

### 3. Results

#### 3.1. Testing and Applying Contact Materials

##### 3.1.1. Heat Test of Contact Materials

Materials that underwent thermal input testing melted 5–10 K higher than that of their specified melting or liquidus points except the SnPb alloy, which exhibited no perceivable changes even when warmed by 30 K above its specified liquidus, except a barely noticeable color change.

A disinclination was noted with all solder alloys adhering to the aluminum substrate regardless of utilization of flux. The solder pieces formed a sphere instead of spreading on the substrate, demonstrating subpar wetting of the surface. The SAC-305 solder piece held onto the substrate in a small area but was effortlessly removed, as no metallurgical bond was established.

The only inspected brazing metal was the Zn-22Al alloy, which spread out on the surface and bonded to the substrate. The brazed fin piece could be bent and held strong without apparent damage to it. Due to the fin having been made of this specific material, other filler metals could not be considered, as part of the fin was destroyed when heating the furnace above 570 °C.

##### 3.1.2. Adhesive

After the specified curing process, the connection was inspected. The joint produced was satisfactory in both adhesions to surfaces as well as mechanical strength for the expected loads, regardless of the joined surfaces having been prepared by grinding and polishing processes. The performance of heat conductivity was lined up to be appraised against other bonding methods upon the successful creation of various uniform specimens of tube and fin.

##### 3.1.3. Soldering and Brazing

The furnace and torch soldering trials ended in virtually the same outcome: the different alloys bonded to the copper surface but did not even wet the aluminum fin and no metallurgical bond was established.

It was observed throughout several production processes that the molten solder would not remain between the pipe and the lamella during gas torch and furnace soldering attempts.

Two brazing attempts were made in the furnace. The outcome was the same: no connection was built, as the filler metal melted at a much higher temperature than expected, and the middle part of the fin was destroyed by the heat.

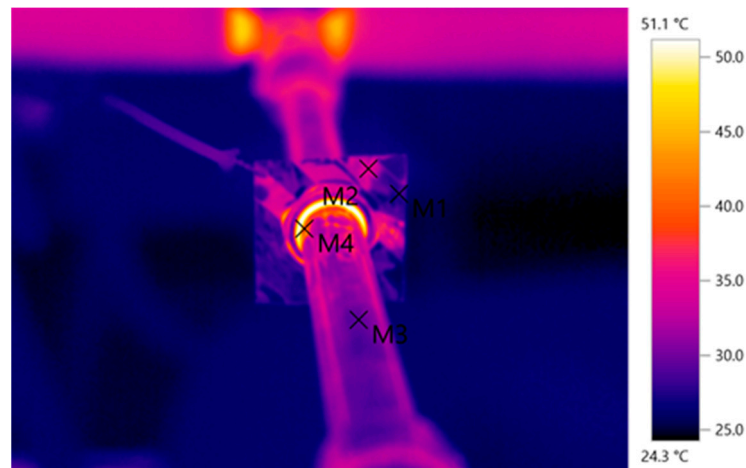
Brazing with the blowtorch was a success, and the proper bond between the fin and the pipe was created with adequate-for-purpose mechanical strength, although a tiny piece of the fin was incinerated, and the surface coating layer was ruined in the small surrounding area.

#### 3.2. Thermal Camera Measurement Results

##### 3.2.1. Measurement Results of 40 mm × 40 mm Fins

During the measurements, problems were encountered, which made it necessary to rethink the experiment. The first problem was that due to reflective surfaces, the surface temperature of the lamella cannot be measured directly by thermography (Figure 5 and Table 2).

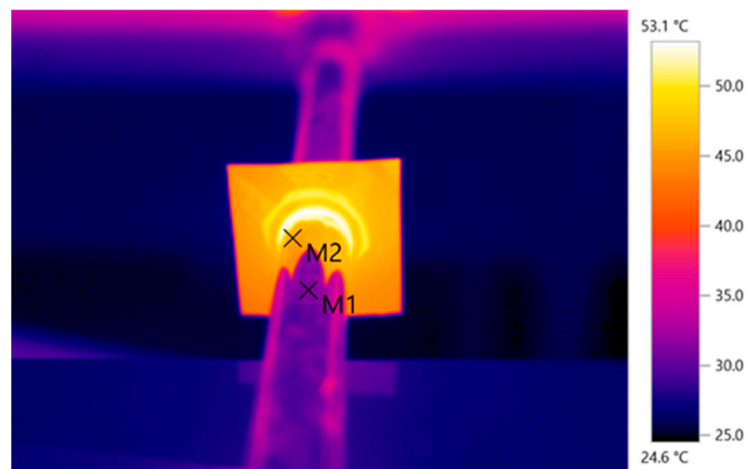
A solution to this problem was to make the surface to be measured matte, which can be achieved by applying a thin layer of paint that does not affect the measured values. Therefore, the lamella and part of the pipe were painted and imaged, as shown in Figure 6. The temperature values are shown in Table 3.



**Figure 5.** Thermal imaging of a specimen with reflective surfaces.

**Table 2.** Inaccurate measurement results due to reflective surface. The reflected temperature is the room temperature.

Measurement Point	Temperature [°C]	Reflected Temperature [°C]
M1	28.0	25.0
M2	34.7	25.0
M3	29.4	25.0
M4	39.2	25.0



**Figure 6.** The difference between a matte-painted surface (brighter yellow-orange) and an unpainted reflective surface (blue-violet).

**Table 3.** Matte-painted and reflective surface temperature measurements.

Measurement Point	Temperature [°C]	Emission	Reflected Temperature [°C]
M1	31.2	-	25.0
M2	46.2	0.95	25.0

For thermal imaging measurements, it is essential to know the emissivity of the surface in order to determine the exact temperature. Since the emissivity of the paint was not known, it was determined after the painted surface was formed. The emissivity of the paint was determined to be  $\epsilon = 0.95$  [-] using an emissivity strip of known parameters.

It is difficult to compare the surface temperatures of the fins measured with a thermal camera because the location of the measurement points and their measured temperatures cannot be determined exactly for each fin. In addition, the problem is that there is only



a minute difference in temperature between the base of the lamellae and the ends of the lamellae, resulting in inaccurate measurements that cannot be compared in this form. A graph is made to compare measurement results, as demonstrated in Figure 7, with thermal images of measured samples shown in Figure 8.

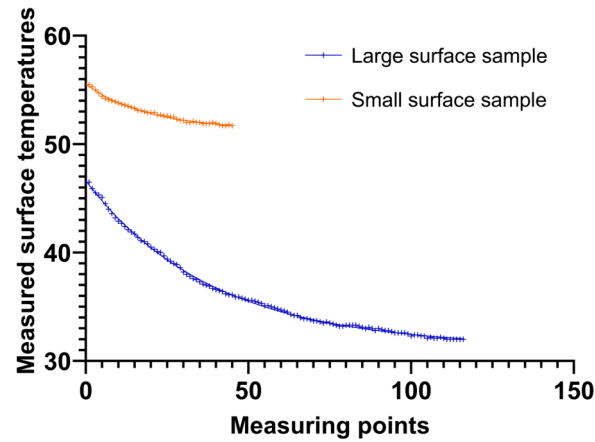


Figure 7. Surface temperature values of the small and the large samples.

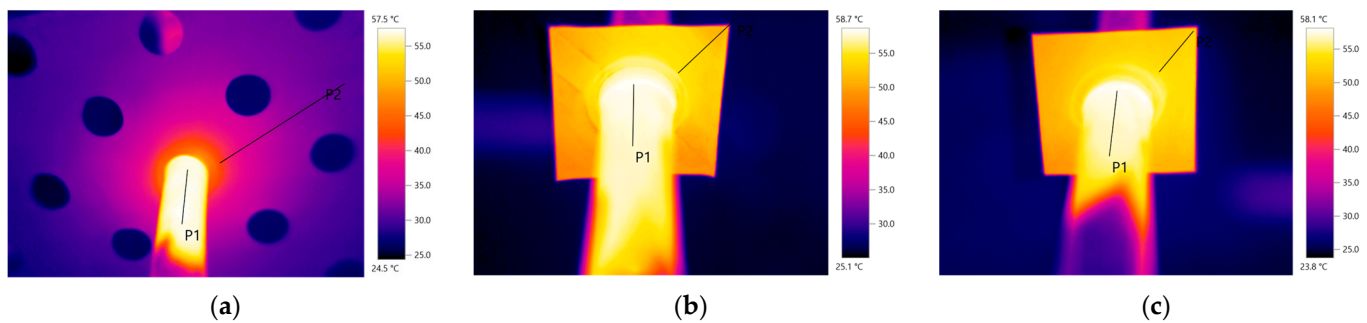
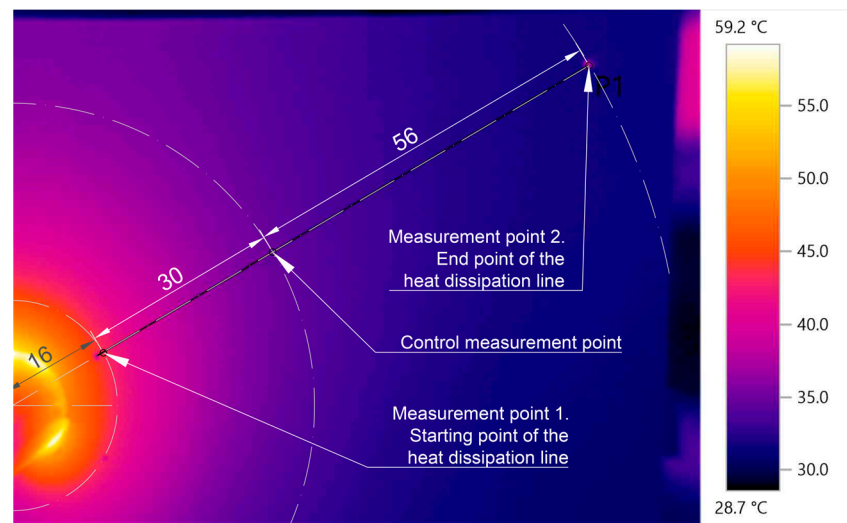


Figure 8. Thermal images of different measurement samples. (a) Large surface sample; (b) Small surface sample 1 (40 mm × 40 mm); (c) Small surface sample 2 (40 mm × 40 mm).

The use of a fan was also considered to achieve a higher heat transfer coefficient so that the temperature difference between the base of the blades and the ends of the blades is higher than the natural airflow. The issue with this added circumstance in the experiment is that it is difficult to ensure the same airflow condition.

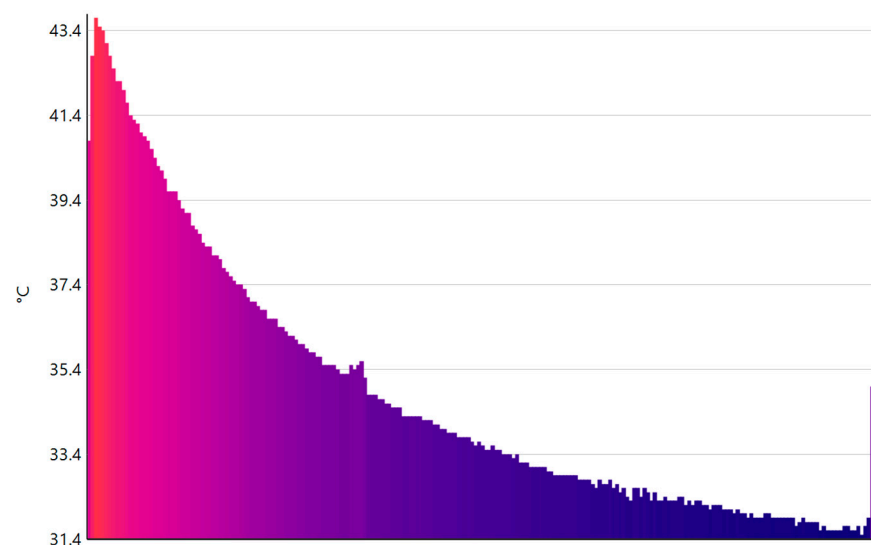
### 3.2.2. Measurement Results of 200 mm × 116 mm Fins

Based on the previous measurement experience, it was necessary to use a larger fin. It is important to note that the larger slat size is not a model of the real situation. The arrangement of the tubes is closer in reality, so a lamella of this size around a single pipe does not exist. However, this approach is suitable to study the effect of heat conduction, as a larger fin size will result in a larger temperature drop. In this case, a tight fit may improve the contact between the tube and the fin, and then there would be better thermal conductivity. Consequently, the temperature difference may rise towards the edge of the fin, compared to a poorer thermal conductivity connection. Two sample fins were prepared for the measurement, one with a loose fit and one with a tight fit. During the measurement, thermal images of the surface of the fins were taken. For a given fin, two thermal images were taken from two angles along a given line, providing a basis for validation and comparison. The measurement line (P1) of the surface temperature was placed at the same location in both fins (Figure 9).



**Figure 9.** Thermal image of the 200 mm × 116 mm lamella and measurement point locations.

To interpret this in the thermal image, a small hole was made in the fin at the start and end points of the line, and a control point was placed between them. This ensures that the line can be placed in the same location for each measurement when processing the thermal image. A histogram is created with the acquired measurement data (Figure 10).



**Figure 10.** Line histogram with temperature values (Minimum: 31.5 °C, Maximum: 43.7 °C, Mean: 34.8 °C).

A statistical method, the Wilcoxon rank sum test, was used to compare the resulting data series. The data series are not normally distributed as they follow a trend, and the comparison of continuous data points is a more expedient method.

The Wilcoxon test is a non-parametric statistical test used to test for differences between two linked samples. There are two variants, more powerful and flexible than parametric tests (*t*-test, etc.), especially when the data are not normally distributed or have a small sample size.

There are two versions of the Wilcoxon test. The Wilcoxon signed-rank test is used to compare paired samples and considers the sign and magnitude of the variances. Wilcoxon rank-sum test is used to compare independent samples, also known as the Mann–Whitney U-test. It is used when two samples are not normally distributed and the sample size is small [27,28]. This latter was applicable in this case.

The results of the application of the statistical methods show that the data series one and two measured from different angles on sample one are statistically different ( $p < 0.001$ ), but this is not relevant as we are dealing with the same sample and the temperature distribution measured in the same straight line. Furthermore, the thermal images were taken with a second offset. The same finding holds for the two data series of sample two ( $p < 0.001$ ). The results show that data set two of sample two and data set one of sample one is identical ( $p = 0.106$ ). This also shows that the plots show congruent curves with the other data sets. Summarizing the results, it can be concluded that no difference or relevant result can be detected with this method. Likely, the measurement accuracy and conditions are not appropriate for this study.

### 3.3. Finite Element Analysis Results

The total heat transfer rate results of the finite element analysis can be seen in Figure 11 for each model type and the realistic model. The results show the values for each inspected contact material and the absence of any contact material using an air gap.



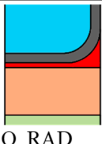



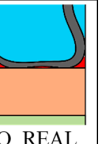
Geometry								
		Q_90	Q_45	Q_RAD	Q_90_NG	Q_45_NG	Q_RAD_NG	Q_REAL
Total heat transfer rate [W]	Sn-9Zn	31.70222	31.126	33.85612	34.90741	34.57142	34.69523	<b>34.81229</b>
	Sn-40Pb	27.79636	31.20424	33.6463	34.90741	34.54353	34.67696	<b>34.77643</b>
	SAC 305	31.91135	31.0724	33.80648	34.90741	34.56401	34.69038	<b>34.80355</b>
	Zn-22Al	31.23269	32.77866	34.36043	34.90741	34.67304	34.75416	<b>34.91314</b>
	Sn-4Ag	31.81301	31.26339	33.75228	34.90741	34.55693	34.6856	<b>34.79408</b>
	Loctite SI5404	17.47187	27.97119	28.58213	34.90741	34.36569	34.49907	<b>34.28268</b>
	Air	0.5575	0.43304	0.5316	34.90741	34.30421	34.3162	<b>33.64973</b>
	Mean difference from the realistic model [W]	9.93527	8.02614	6.21379	0.33307	0.27543	0.21143	

Figure 11. Total heat transfer rate values of the models for each contact material and air in Watts.

There is a marked difference in total heat transfer rate between the idealized and the realistic models in case of an air gap. This difference is demonstrated in Figure 12.

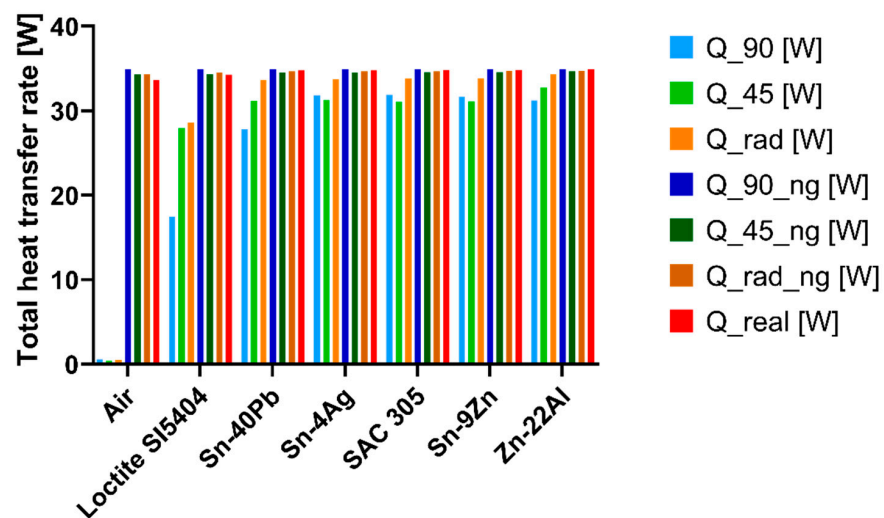


Figure 12. Total heat transfer rate by geometries and contact materials.

It is demonstrated that the models with no gap between the fin and tube provide closer results to the realistic models than the others. Thus, after further inspection of these results, the models with the gap are neglected. The relation between the thermal conductivity of the contact material and the simulated heat transfer rate can be an important thing to investigate. This relationship is shown in Figure 13.

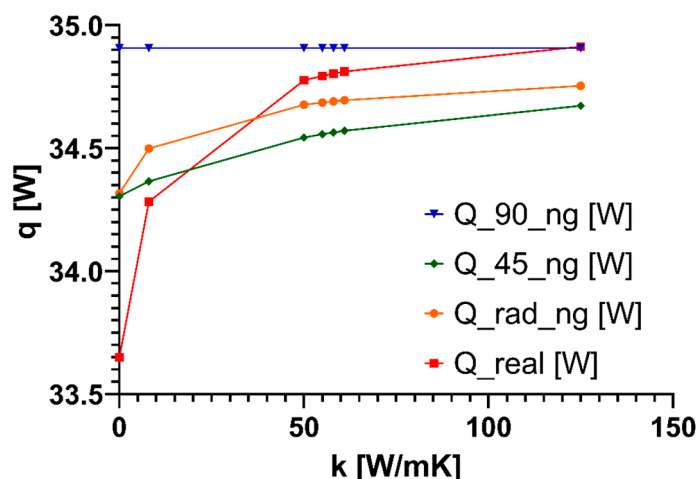


Figure 13. Heat transfer rate as the factor of thermal conductivity of the contact materials.

#### 4. Discussion

A few heat-tested solder alloys behaved unpredictably in the furnace. Examples include but are not limited to a piece remaining solid despite temperatures reaching well over its stated liquidus point, only a slight darkening of the surface being apparent.

Possible explanations for this phenomenon were considered, and the following conclusions were entertained:

- One alloy piece was contorted several times, which could have left stresses inside the material, changing some of its properties;
- A second piece was from an older soldering wire; it may have been mishandled or held in storage improperly, allowing the surface to oxidize or be fouled with contaminants;
- During one of the tests, flux was applied to the substrate after the solder piece was placed on it. The flux may have changed the chemistry of the surface layer of the solder segment, which resulted in this layer remaining solid despite the elevated temperatures.

Our trials concluded with a failure to solder copper to aluminum and a partially successful brazing attempt.

The potential causes for the unsuccessful soldering processes were

- Improper grit sandpaper was used during preparation;
- Used fluxes were ineffective;
- Aluminum oxide;
- Execution inadequately planned or performed;
- Too large gap size between pipe and fin;
- Used soldering methods allowed oxidization during the processes;
- Contaminated surface of solders or substrates (grease, dust, oxides);
- The slow manual process allows for the growth of aluminum oxide on the surface of the fin after grinding, even in the few seconds it took to apply flux;
- The used aluminum alloy is not good for soldering;
- Not enough time left for diffusion;
- Equipment not up to par for the conducted study.

Diffusion takes more time than the time the test samples were kept at said temperature, which would be essential for a soldered bond without an immediate metallurgical bond forming between the solder and substrate.

Literature also confirms that there is an optimal gap size for soldering, which differs between different solder alloys on each distinct substrate, depending on the wetting angle [21].

The brazing was successful using the gas torch, but the fin was slightly burnt. This could be avoided by slowing down the process and managing heat input better or using a slightly lower aluminum content alloy with lower solidus and liquidus temperatures, requiring lower working temperatures.

The finite element analysis demonstrated the effectiveness of the use of contact materials in the case of marked gap formation between the fin and tube of heat exchangers. The results show that if the gap size is negligible, these contact materials make very little difference in heat transfer. Thus, the use of these materials is only feasible if the gap formation is proven. The discovery of this phenomenon is part of further research. Furthermore, the results show that for models with air gaps, the difference in the calculated heat flux compared to the real geometry is striking; therefore, using models without a gap provides more accurate results.

For solder materials with higher thermal conductivity, the model with a 45° corner is the most accurate, while for materials with a lower thermal conductivity (glue, air gap), the model with a radius corner is the most accurate, but 45° is also nearly as accurate. Therefore, for simulation purposes, the most accurate and practical model is the one with a 45° chamfer. It is also easier to use in FEA than the radius model, as it eliminates the well-known meshing problem where the material at the radius gradually reaches 0 thickness.

Figure 13 shows that for materials with a coefficient of thermal conductivity between 0 and 50 W/mK, none of the models follow the real model curve exactly, but above that, they do. This discrepancy is because, in the real model, there is very little contact material between the fin and the tube. This means a high resistance in case of an air gap, which is not the case for models without gaps. In the models with a gap, however, this discrepancy is too large.

Regarding the contact material, it is confirmed that even silicone adhesive is much better than air gap; even with a coefficient of thermal conductivity of around ~1 W/mK, it makes a big difference, as it is still a lot better than the thermal conductivity of air, which is 0.0242 W/mK. The use of contact materials with a thermal conductivity higher than ~50 W/mK is unnecessary and does not significantly increase the heat flux.

#### *Further Research*

Although the heat transfer efficiency may not be significantly impacted by small variations in tube–fin contact materials or gaps, further research should investigate how these modifications can positively influence the lifespan of the heat exchangers. Initial findings suggest that while heat transfer power remains relatively stable, certain materials or design adjustments could enhance durability [29] and resistance to environmental factors, such as types of corrosion or gap deformation. Future studies should focus on how these materials can contribute to extending the operational life of heat exchangers [30] without compromising heat transfer; therefore, further trials also need to look into the resistance of applied contact materials to vibration effects at operating temperatures of a heat exchanger, as well as resistance to heat cycling.

All soldering attempts, save for vacuum chamber soldering, mandate using flux when working on aluminum; therefore, the acquisition of varying types of fluxes could be beneficial if soldering and brazing of these parts are to be further researched in the future.

As the investigated type of heat exchangers are composed of dissimilar metals that are usually electrically connected (metal-to-metal contact exists), especially Cu and an Al-alloy, examination of the parts for galvanic or other types of corrosion could be valuable [31,32].



Other aspects for planned future research:

- Different base materials, better-chosen form, and dimensions;
- Other contact materials (graphite; HC greases, pastes, composites, ZnAl alloy with lower Al content, nanotechnology [33]);
- Contact forming methods (TIG Imp., Sintering, CMT, ECP);
- Production and examination of cross-sections;
- Continuation of studying literature.

## 5. Conclusions

In this study, the thermal performance of various tube–fin contact materials in heat exchangers was assessed using experimental and finite element analysis (FEA) methods. Our findings indicated that contact materials with higher thermal conductivity showed better heat transfer rates compared to those with lower thermal conductivity, such as adhesives. However, even the lower thermal conductivity contact materials increased their heat transfer rates relative to an air gap. The use of Zn-22Al for brazing produced promising results, while soldering attempts faced several challenges due to material incompatibilities.

The FEA results showed the importance of minimizing the air gap between the fin and the tube, as even small gaps can significantly reduce heat transfer efficiency. This was particularly evident in the models where an air gap was present, which led to a significant decrease in heat transfer.

Despite the limitations in soldering and thermal camera measurements, the results enable further exploration into contact materials and their long-term impact on heat exchanger efficiency and lifespan. Moving forward, additional testing with alternative materials and refined methodologies could offer more reliable solutions for improving heat transfer in industrial heat exchangers.

In conclusion, while this research provides a solid foundation for improving heat exchanger design and power, further investigations are needed to refine the use of contact materials, particularly in overcoming soldering challenges and optimizing the brazing processes. By addressing these areas, future developments in heat exchanger technology could lead to more efficient, durable, and sustainable solutions for a wide range of industrial applications.

**Author Contributions:** Conceptualization, L.B. and G.F.V.; methodology, L.B., D.C. and Z.M.; software, D.C.; validation, L.B.; formal analysis, G.L. and L.B.; resources, M.B.; data curation, L.B., G.L. and D.C.; writing—original draft preparation, D.C., T.B., B.K., L.B. and G.F.V.; writing—review and editing, D.C. and B.K.; visualization, L.B., B.K. and D.C.; supervision, M.B., B.C., L.L., T.Z. and G.G.V.; project administration, G.G.V. and G.F.V.; funding acquisition, G.G.V. and G.F.V. All authors have read and agreed to the published version of the manuscript.

**Funding:** This research was funded by Economic Development and Innovation. Operational Programme Plusz of the Ministry of Finance GINOP-Plusz-2.1.1-21-2022-00113. The APC was funded by the Faculty of Engineering at the University of Pécs, Hungary, within the framework of the ‘Call for Grant for Publication (3.0)’.

**Data Availability Statement:** The original contributions presented in the study are included in the article, further inquiries can be directed to the corresponding author.

**Acknowledgments:** The authors would like to express their gratitude to Castolin Zrt. for the solder materials used in this research. Special thanks to Márk Schneider, an engineer at Castolin Zrt. for his assistance in selecting the appropriate solder materials and advising soldering and brazing technologies. The authors also extend their thanks to Henkel Magyarország Ltd. for donating the adhesive materials, and to Péter Bakai for providing expert guidance on adhesive technologies. The authors acknowledge the support from Bálint Babits and Ferenc Gábor from CAADEX Ltd. as well as the team at eCon Engineering Ltd., for their professional consultations which contributed to the heat exchanger measurement tasks and Ansys simulations. Special thanks to Ákos Cvenits and Viktor Reisz, laboratory technicians at the University of Pécs FEIT, for their help in preparing the tube–fin samples.

**Conflicts of Interest:** The authors declare no conflicts of interest. The funders had no role in the design of the study; in the collection, analyses, or interpretation of data; in the writing of the manuscript; or in the decision to publish the results.

## References

1. Zaib, F.; Ganesan, P.; Zaharinie, T.; Chen, Z.; Naganthran, K. Heat Transfer Performance of a Compact Heat Exchanger Based on Metal Foam and Thermal Interface Material (TIM). *Int. J. Heat Mass Transf.* **2024**, *231*, 125861. [[CrossRef](#)]
2. Rădulescu, S.; Negoitǎ, L.I.; Onuțu, I. Analysis of the Heat Transfer in Double and Triple Concentric Tube Heat Exchangers. In *IOP Conference Series: Materials Science and Engineering*; IOP Publishing: Bristol, UK, 2016; Volume 147.
3. Jeong, J.; Kim, C.N.; Youn, B. A Study on the Thermal Contact Conductance in Fin-Tube Heat Exchangers with 7 Mm Tube. *Int. J. Heat Mass Transf.* **2006**, *49*, 1547–1555. [[CrossRef](#)]
4. Hing, Y.K.; Raghavan, V.R.; Meng, C.W. Investigation of Contact Resistance for Fin-Tube Heat Exchanger by Means of Tube Expansion. In *AIP Conference Proceedings*; American Institute of Physics: College Park, MD, USA, 2012; Volume 1440.
5. Fletcher, L.S.; Gyorog, D.A. *Heat Transfer Between Surfaces in Contact: An Analytical and Experimental Study of Thermal Contact Resistance of Metallic Interfaces*; NASA: Tempe, AZ, USA, 1971.
6. Kiatpachai, P.; Kaewkamrop, T.; Mesgarpour, M.; Ahn, H.S.; Dalkılıç, A.S.; Mahian, O.; Wongwises, S. Air-Side Performance of Embedded and Welded Spiral Fin and Tube Heat Exchangers. *Case Stud. Therm. Eng.* **2022**, *30*, 101721. [[CrossRef](#)]
7. Han, C.; Sin, I.; Kwon, H.; Park, S. The Role of the Process and Design Variables in Improving the Performance of Heat Exchanger Tube Expansion. *Appl. Sci.* **2018**, *8*, 756. [[CrossRef](#)]
8. Tang, D.; Li, D.; Peng, Y. Optimization to the Tube-Fin Contact Status of the Tube Expansion Process. *J. Mech. Work. Technol.* **2011**, *211*, 573–577. [[CrossRef](#)]
9. Saltarelli, R.; Alves, L.M.; Fasano, M.; Afonso, R.M. Joining by Forming Technology for Thermal Applications: A Case Study of Finned Tube Heat Exchanger. *Case Stud. Therm. Eng.* **2024**, *59*, 104551. [[CrossRef](#)]
10. Scattina, A. Numerical Analysis of Tube Expansion Process for Heat Exchangers Production. *Int. J. Mech. Sci.* **2016**, *118*, 268–282. [[CrossRef](#)]
11. Stubblefield, M.A.; Pang, S.S.; Cundy, V.A. Heat Loss in Insulated Pipe—The Influence of Thermal Contact Resistance: A Case Study. *Compos. Part B Eng.* **1996**, *27*, 85–93. [[CrossRef](#)]
12. Orżanowski, T.; Madura, H. Test and Evaluation of Reference-Based Nonuniformity Correction Methods for Microbolometer Infrared Detectors. *Opto-Electron. Rev.* **2010**, *18*, 91–94. [[CrossRef](#)]
13. Krupiński, M.; Bieszczad, G.; Sosnowski, T.; Madura, H.; Gogler, S. Non-Uniformity Correction in Microbolometer Array with Temperature Influence Compensation. *Metrol. Meas. Syst.* **2014**, *21*, 709–718. [[CrossRef](#)]
14. Budulski, L. *Measurement Technology and Building Diagnostics*; University of Pécs: Pécs, Hungary, 2021.
15. Taler, D.; Taler, J. Steady-State and Transient Heat Transfer through Fins of Complex Geometry. *Arch. Thermodyn.* **2014**, *35*, 117–133. [[CrossRef](#)]
16. Blechich, P.; Trp, A.; Lenić, K. Thermal Performance Analysis of Fin-and-Tube Heat Exchangers Operating with Airflow Nonuniformity. *Int. J. Therm. Sci.* **2021**, *164*, 106887. [[CrossRef](#)]
17. Chávez-Modena, M.; González, L.M.; Valero, E. Numerical Optimization of the Fin Shape Experiments of a Heat Conjugate Problem Surface Air/Oil Heat Exchanger (SACOC). *Int. J. Heat Mass Transf.* **2022**, *182*, 121971. [[CrossRef](#)]
18. Kim, K.R.; Lee, J.K.; Jeong, H.D.; Kang, Y.H.; Ahn, Y.C. Numerical and Experimental Study of Air-to-Air Plate Heat Exchangers with Plain and Offset Strip Fin Shapes. *Energies* **2020**, *13*, 5710. [[CrossRef](#)]
19. Ciuffini, A.; Scattina, A.; Carena, F.; Roberti, M.; Toscano Rivalta, G.; Chiavazzo, E.; Fasano, M.; Asinari, P. Multiscale Computational Fluid Dynamics Methodology for Predicting Thermal Performance of Compact Heat Exchangers. *J. Heat Transf.* **2016**, *138*, 071801. [[CrossRef](#)]
20. Lindqvist, K.; Skaugen, G.; Meyer, O.H.H. Plate Fin-and-Tube Heat Exchanger Computational Fluid Dynamics Model. *Appl. Therm. Eng.* **2021**, *189*, 116669. [[CrossRef](#)]
21. Mirski, Z.; Granat, K.; Drzeniek, H.; Piwowarczyk, T.; Wojdat, T. Soldering of Aluminium with Copper. *Weld. Int.* **2013**, *27*, 190–195. [[CrossRef](#)]
22. Merlin, K.; Delaunay, D.; Soto, J.; Traonvouez, L. Heat Transfer Enhancement in Latent Heat Thermal Storage Systems: Comparative Study of Different Solutions and Thermal Contact Investigation between the Exchanger and the PCM. *Appl. Energy* **2016**, *166*, 107–116. [[CrossRef](#)]
23. Kim, C.N.; Jeong, J.; Youn, B.; Kil, S.H. An Experimental-Numerical Evaluation of Thermal Contact Conductance in Fin-Tube Heat Exchangers. *JSME Int. J. Ser. B Fluids Therm. Eng.* **2003**, *46*, 299–307. [[CrossRef](#)]
24. Wilcox, D.C. *Turbulence Modeling for CFD*, 3rd ed.; DCW Industries: La Canada, CA, USA, 2006.
25. Menter, F.R. Two-Equation Eddy-Viscosity Turbulence Models for Engineering Applications. *AIAA J.* **1994**, *32*, 1598–1605. [[CrossRef](#)]
26. *Fluent Theory Guide Ansys Fluent Theory Guide*; ANSYS Inc.: Canonsburg, PA, USA, 2013; Volume 15317, pp. 724–746.
27. Krishnamoorthy, K. Wilcoxon Signed-Rank Test. In *Handbook of Statistical Distributions with Applications*; Chapman and Hall/CRC: London, UK, 2020.
28. Wilcoxon, F. Individual Comparisons by Ranking Methods. *Biom. Bull.* **1945**, *1*, 80–270. [[CrossRef](#)]

29. Patel, A. Heat Exchanger Materials and Coatings: Innovations for Improved Heat Transfer and Durability. *Anand Patel. Int. J. Eng. Res. Appl.* **2023**, *13*, 131–142.
30. Faes, W.; Lecompte, S.; Ahmed, Z.Y.; Van Bael, J.; Salenbien, R.; Verbeken, K.; De Paepe, M. Corrosion and Corrosion Prevention in Heat Exchangers. *Corros. Rev.* **2019**, *37*, 131–155. [[CrossRef](#)]
31. Wang, Z.; Li, H.; Cheng, D.; Qin, S.; Li, D.; Zhang, X. A Laboratory Study of the Failure Analysis of Copper Tube Used in the Air Conditioning Heat Exchanger. *Mater. Corros.* **2024**, *75*, 924–931. [[CrossRef](#)]
32. Cozzarini, L.; Marsich, L.; Schmid, C. Ant-Nest Corrosion Failure of Heat Exchangers Copper Pipes. *Eng. Fail. Anal.* **2020**, *109*, 104387. [[CrossRef](#)]
33. Van Heerden, D.; Rude, T.R.; Newson, J.; He, J.; Besnoin, E.; Knio, O.M.; Weihs, T.P. A Tenfold Reduction in Interface Thermal Resistance for Heat Sink Mounting. *J. Microelectron. Electron. Packag.* **2004**, *1*, 187–193. [[CrossRef](#)]

**Disclaimer/Publisher’s Note:** The statements, opinions and data contained in all publications are solely those of the individual author(s) and contributor(s) and not of MDPI and/or the editor(s). MDPI and/or the editor(s) disclaim responsibility for any injury to people or property resulting from any ideas, methods, instructions or products referred to in the content.